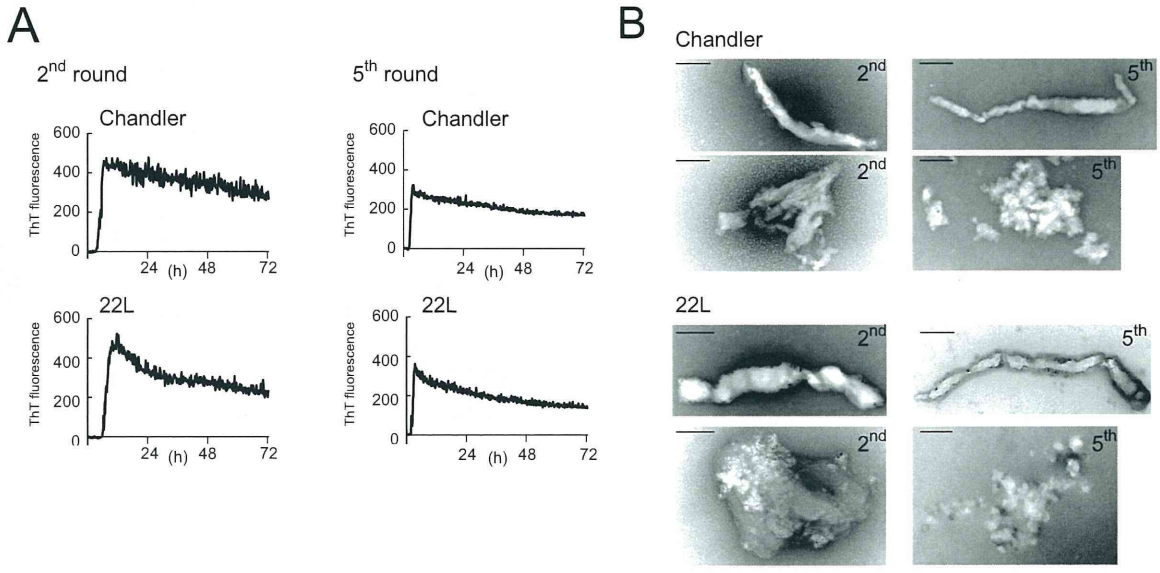

FIG 2 Formation of PrP^{Sc}-seeded rPrP fibrils in the 2nd round (2nd-rPrP-fib^{Sc}) and 5th round (5th-rPrP-fib^{Sc}) of RT-QUIC. (A) Between each round, the reaction mixtures from the previous reaction were diluted 100-fold into fresh rPrP. The reaction buffer contained 300 mM NaCl, 50 mM HEPES (pH 7.5), and 10 μM ThT. The rPrP concentration was 100 μg/ml. (B) TEM analysis of PrP^{Sc}-seeded rPrP fibrils generated in the second and fifth rounds of RT-QUIC. Bars, 100 nm.

which was markedly higher than that of 1st-rPrP-fib^{Sc} (Fig. 5B and Table 1). Additionally, we tested the conformational stability of 2nd- and 5th-rPrP-fib^{Sc} but found no significant differences between strains (Fig. 5C and D and Table 1).

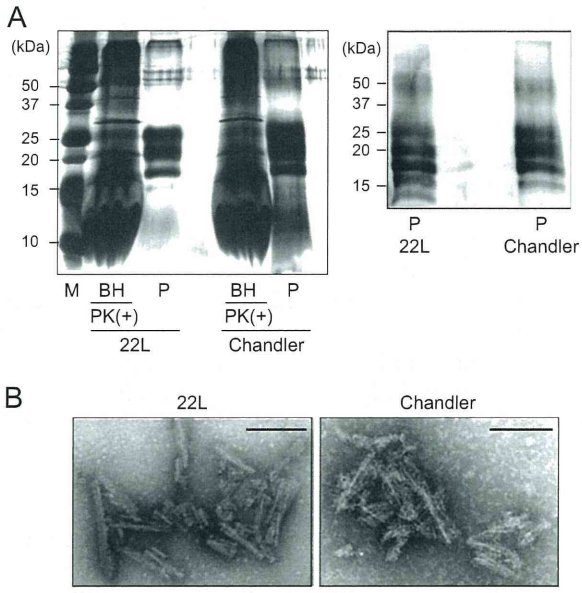

FIG 3 Silver staining and Western blot analysis of purified PrP^{Sc}. (A) The purified PrP^{Sc} samples (P) were examined by silver-stained SDS-polyacrylamide gel analysis (left). For comparison, the electrophoretic pattern of prion-infected BHs containing 100 μg total protein digested with PK (20 μg/ml, 37°C for 1 h) is shown (left). The purified PrP^{Sc} samples were immunoblotted with polyclonal anti-PrP antibody M20 (right). Molecular mass markers (lane M) are indicated in kilodaltons (kDa) on the left side of each panel. (B) Electron microscopy analysis of purified 22L PrP^{Sc} (left) and Chandler PrP^{Sc} (right). Bars, 100 nm.

Bioassay for rPrP fibrils generated in QUIC reactions. To determine whether the infectivity was transmitted to the rPrP fibrils, we performed a bioassay using wild-type mice. To prepare the control materials, seed-only solutions containing the same concentration of PrP^{Sc} as that in 1st- or 5th-rPrP-fib^{Sc} were subjected to a mock RT-QUIC procedure and then mixed with the same amount of soluble rPrP (Table 2). The survival periods of mice inoculated with 40-μl aliquots containing rPrP fibrils were 185.5 ± 4.0 days postinoculation (dpi) for 1st-rPrP-fib^{Ch} and 213.0 ± 8.9 dpi for 1st-rPrP-fib^{22L} (Table 2). In contrast, the attack rate of these control mice was only 50% (2/4) for Chandler and 20% (1/5) for 22L. Moreover, the survival period of the affected mice was much longer than that of the mice inoculated with 1st-rPrP-fib^{Sc} (Table 2). For comparison with the 50% lethal dose (LD_{50}) of the original PrP^{Sc}, the LD_{50} of 1st-rPrP-fib^{Sc} was determined from the linear regression relationship between infectious titers and survival periods. The infectious titers (per 40 μl) of 1st-rPrP-fib^{Ch} and 1st-rPrP-fib^{22L} were estimated to be 407.2 ± 226.6 and 1,067.0 ± 678.7 LD_{50}s, respectively, whereas the titers of the Chandler and 22L prions were 20.2 and 28.9 LD_{50} units/40 pg of PrP^{Sc}, respectively. Because the QUIC reaction in the first round resulted in a 20- to 37-fold increase in the infectious titer, the seed contribution to infectivity is estimated to be about 3 to 5%. In contrast, none of the mice inoculated with 5th-rPrP-fib^{Sc} developed symptoms related to TSE (Table 2), suggesting that the 5th-rPrP-fib^{Sc} has no substantial infectivity.

We analyzed by Western blotting the levels of PrP^{Sc} in the brain tissues of mice in the terminal stage that had been inoculated with 1st-rPrP-fib^{Sc} or control materials (mock 1st QUIC) and found no apparent differences in the accumulation of PrP^{Sc} between them and mice inoculated with mock 1st QUIC (Fig. 6A). In addition, a conformational stability assay with GdnHCl revealed that the strain-specific digestion pattern was preserved in mice inoculated with 1st-rPrP-fib^{Sc} (Fig. 6B).

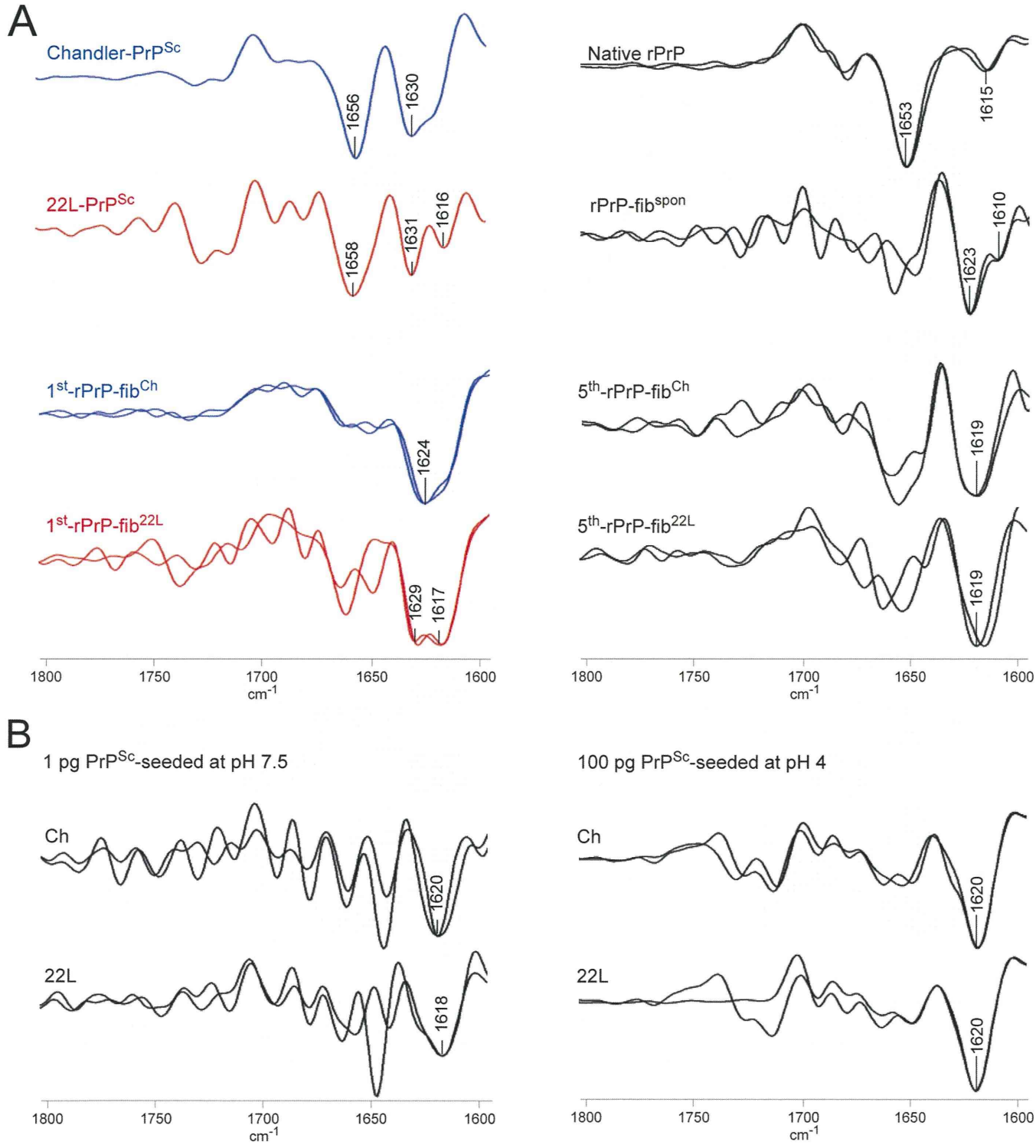

FIG 4 FTIR spectroscopic characterization of rPrP fibrils and purified PrP^{Sc}. (A) Second-derivative FTIR spectra are shown for purified PrP^{Sc}, 1st-rPrP-fib^{Sc}, 5th-rPrP-fib^{Sc}, spontaneously formed rPrP fibrils (rPrP-fib^{spon}), and native rPrP. Overlaid spectra are from independent preparations. (B) FTIR spectra of rPrP fibrils generated at pH 7.5 in the presence of a small amount (1 pg) of PrP^{Sc} and rPrP fibrils generated at pH 4 in the presence of 100 pg of PrP^{Sc}.

Next, the degree of vacuolation in brain sections, including the hippocampus (HI), cerebral cortex, thalamus, pons, and cerebellum (CE), from affected mice inoculated with 1st-rPrP-fib^{Sc} or mock 1st QUIC and those inoculated with the second passage of 1st-rPrP-fib^{Sc} was examined histologically (Fig. 6C and D). Of note, we found that the spongiform change in mice inoculated with 1st-rPrP-fib^{Sc} was less severe in the HI and CE than that in the HI and CE of mice inoculated with mock 1st QUIC strains (Fig. 6C

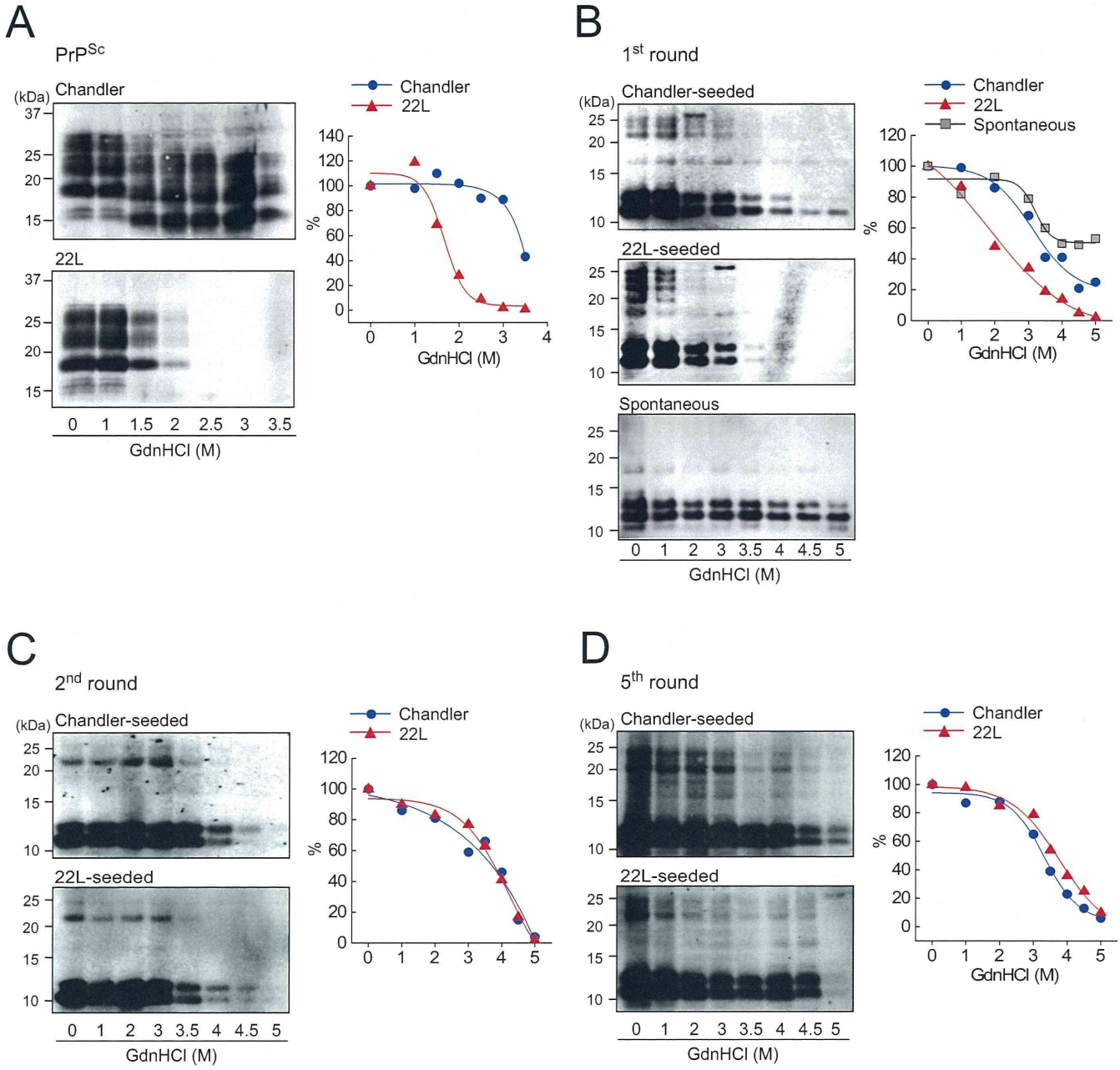

FIG 5 Conformational stability assay for PrP^{Sc} in BH and rPrP fibrils. (A) Chandler-infected (top left) or 22L-infected (bottom left) BHs were treated with 0 to 3.5 M GdnHCl and subjected to PK digestion. PrP^{Sc} was detected by R20 anti-PrP polyclonal antibody. The denaturation curves were plotted using Boltzmann curve fitting (right). (B to D) PK-digested 1st-rPrP-fib^{Sc} (generated as described in the legend to Fig. 1) and rPrP-fib^{spon} (B), 2nd-rPrP-fib^{Sc} (C), or 5th-rPrP-fib^{Sc} (D) were analyzed by Western blotting following GdnHCl treatment (0 to 5 M). The PK-resistant fragments of the rPrP fibrils were detected by antibody R20.

TABLE 1 Conformational stabilities of purified PrP^{Sc} and rPrP fibrils[a]

Strain	$[GdnHCl]_{1/2}$ (mol/liter)			
	Purified PrP^{Sc}	rPrP fibrils		
		1st	2nd	5th
Chandler	3.3 ± 0.4**	3.3 ± 0.1*	3.7 ± 0.1	3.3 ± 0.3
22L	1.7 ± 0.3	2.3 ± 0.6	3.8 ± 0.2	3.5 ± 1.0
Spontaneous		>5		

[a] The $[GdnHCl]_{1/2}$ values (mol/liter) are means ± standard deviations from three independent experiments. Statistical significance was determined using one-way ANOVA, followed by Student's *t* test. **, $P < 0.01$ (compared with 22L); *, $P < 0.05$ (compared with 22L).

and D). Furthermore, these different lesion profiles observed in mice inoculated with 1st-rPrP-fib^{Sc} were preserved upon second passage (Fig. 6D), suggesting that the characters of 1st-rPrP-fib^{Sc} are partially distinct from those of the original strains. These findings support the notion that 1st-rPrP-fib^{Sc} provoke the emergence of a mutant strain beyond seed-derived infectivity.

DISCUSSION

Recent studies show that RT-QUIC assays are useful for the sensitive detection of PrP^{Sc} in most species and strains, including

TABLE 2 Bioassay for rPrP fibrils generated in QUIC reactions in wild-type mice[a]

Inoculum	Concn of seed PrP^{Sc} (pg/μl)	Survival period (dpi)[b]	Mortality (no. of dead mice/ total no. tested)
1st-rPrP-fib^{Ch}	1	185.5 ± 4.0**[d]	4/4
Mock 1st QUIC (Ch)[c]	1	201, 220[e]	2/4
1st-rPrP-fib^{22L}	1	213.0 ± 8.9**[d]	6/6
Mock 1st QUIC (22L)[c]	1	333[e]	1/5
5th-rPrP-fib^{Ch}	1×10^{-8}	>660[f]	0/4
Mock 5th QUIC (Ch)[c]	1×10^{-8}	>660[f]	0/4
5th-rPrP-fib^{22L}	1×10^{-8}	>660[f]	0/6
Mock 5th QUIC (22L)[c]	1×10^{-8}	>660[f]	0/6
rPrP-fib^{spon}	0	>660[f]	0/6
Second passage of 1st-rPrP-fib^{Ch}		152.0 ± 8.5[d]	5/5
Second passage of mock 1st QUIC (Ch)[g]		148.4 ± 5.9[d]	5/5
Second passage of 1st-rPrP-fib^{22L}		153.5 ± 0.6[d]	5/5
Second passage of mock 1st QUIC (22L)[h]		149.6 ± 10.4[d]	4/4

[a] Mice were intracerebrally inoculated with 40 μl of each inoculum. For the second passage, 10% BH was used.
[b] Statistical significance was determined using the log rank test. **, $P < 0.01$ (compared with the controls); *, $P < 0.05$ (compared with the controls). dpi, days postinoculation.
[c] After subjecting seed-only mixtures containing the same concentration of PrP^{Sc} as 1st- or 5th-rPrP-fib^{Sc} to a mock QUIC procedure, the same amount of rPrP was added. The solutions were inoculated into mice as controls for rPrP fibrils.
[d] Data represent means ± standard deviations.
[e] Data represent the survival periods of the TSE-positive mice. All nonsymptomatic mice were negative for PrP^{Sc} at 660 dpi.
[f] Data represent the day postinoculation when the experiment was ended.
[g] A sample from a mouse obtained at 201 dpi was used.
[h] A sample from a mouse obtained at 333 dpi was used.

Creutzfeldt-Jakob disease (CJD) in humans (28, 35–37), scrapie in rodents (29, 38), and chronic wasting disease (CWD) in cervids (39). In the RT-QUIC reaction, soluble rPrP is converted to amyloid fibrils in a seed-dependent fashion in the presence of PrP^{Sc}. Previous studies using FTIR and hydrogen-deuterium exchange have shown that there are structural differences between PrP^{Sc}-seeded fibrils and spontaneous rPrP fibrils generated in rPrP amplified by PMCA (7, 40). We also found that the structural morphology (Fig. 1C), secondary structure (Fig. 3), and conformational stability (Fig. 4B and Table 1) distinguish 1st-rPrP-fib^{Sc} from rPrP-fib^{spon}. However, it has been unknown whether rPrP retains the conformational properties of the original PrP^{Sc} in the RT-QUIC. Consistent with previous reports (7, 11), we observed strain differences in the β-sheet structure and conformational stability of PrP^{Sc} between the Chandler and 22L strains. Likewise, the differences in the shape of the β-sheet spectrum between strains were common to both PrP^{Sc} and 1st-rPrP-fib^{Sc}. Furthermore, the conformational stability of 1st-rPrP-fib^{22L} was significantly lower than that of 1st-rPrP-fib^{Ch}, as was the case with Chandler and 22L PrP^{Sc}. Since the original PrP^{Sc} remaining in 1st-rPrP-fib^{Sc} was equivalent to only about 0.01 to 0.02% of the PK-resistant 1st-rPrP-fib^{Sc} (1 to 2 μg/10 μg of total PrP) in our estimation, the contribution to the FTIR spectra and the conformational stability of 1st-rPrP-fib^{Sc} are considered to be negligible. Taken together, these studies demonstrate that at least some strain-specific conformational features, especially in the β-sheet region, are conserved between PrP^{Sc} and 1st-rPrP-fib^{Sc}. However, these unique structural features disappeared in subsequent rounds.

One of the reasons for the loss of strain specificity may be due to differences between *E. coli*-derived rPrP and brain-derived PrP^{C}. Studies using circular dichroism and ^{1}H nuclear magnetic resonance spectroscopy showed that the tertiary structure and the thermal stability of bovine rPrP from positions 23 to 230 are essentially identical to those of healthy calf brain-derived PrP^{C} (41). However, it should be noted that *E. coli*-derived rPrP lacks posttranslational modifications of PrP^{C}, such as glycosylation and a glycosylphosphatidylinositol (GPI) anchor. PrP has two N-linked glycosylation sites at amino acids 180 and 196, resulting in di-, mono-, and unglycosylated forms. Mature PrP^{C} is rich in the diglycosylated form, whereas the glycoform ratio of PrP^{Sc} is known to vary among strains (42–44). Studies using PrP glycan-lacking Tg mice revealed that the strain-specific characteristics of strain 79A were affected by the glycosylation status of PrP^{C}, but those of strains ME7 and 301C were not (45). Meanwhile, enzymatic deglycosylation of PrP^{C} failed to affect strain-specific pathological changes in serial PMCA experiments seeded with two murine strains, RML and 301C (46). However, the same two strains were converted into a new single strain during serial rPrP-PMCA in the presence of synthetic PE (27). Similarly, the emergence of mutant strains whose lesion profiles differed from the lesion profile of the seed strain was also observed in a bioassay using hamster rPrP fibrils generated in seeded rPrP-PMCA (25) or 1st-rPrP-fib^{Sc} (Fig. 6C and D). These results raise the possibility that the lack of a GPI anchor in rPrP leads to alterations in strain-specific characteristics. Furthermore, the cell tropisms determined by the cell panel assay were altered in strains RML, 139A, 79A, and ME7 but not in strain 22L when the strains were propagated in Tg mice expressing PrP devoid of a GPI anchor (47). These studies demonstrate that glycosylation and a GPI anchor are not necessarily required for the propagation of prion infectivity but can influence the strain properties. Although the molecular basis of the emergence of mutant strains remains elusive, we can speculate that the posttranslational changes to PrP might affect the conformation of PrP^{Sc} or the interaction with some cofactor(s) in a strain-specific manner.

Another possible explanation is that nonspecific rPrP fibrils are generated during the serial RT-QUIC and replicate more rapidly than the fibrils with strain-specific conformations. The term "nonspecific rPrP fibrils" arises from our findings that there was little difference in the infrared spectra and conformational stability of 5th-rPrP-fib^{Sc} between strains. It has been reported that the propagation of prion strains in cells cultured under different environmental conditions often leads to the formation of quasispecies that are assumed to be composed of a variety of conformational variants (48, 49). Once generated, the competition among the variants is thought to occur during propagation. Indeed, two conformational variants of rPrP fibrils have been shown to be mutually exclusive and compete for monomeric rPrP as a substrate in fibril formation (30). Furthermore, competitive amplification of two prion strains was demonstrated by BH-PMCA (50). Similarly, nonspecific rPrP fibrils would be expected to become the majority if they had a selective growth advantage in the RT-QUIC. We found that the β-sheet spectra of rPrP fibrils generated in the presence of a small amount (1 pg) of PrP^{Sc} or rPrP fibrils

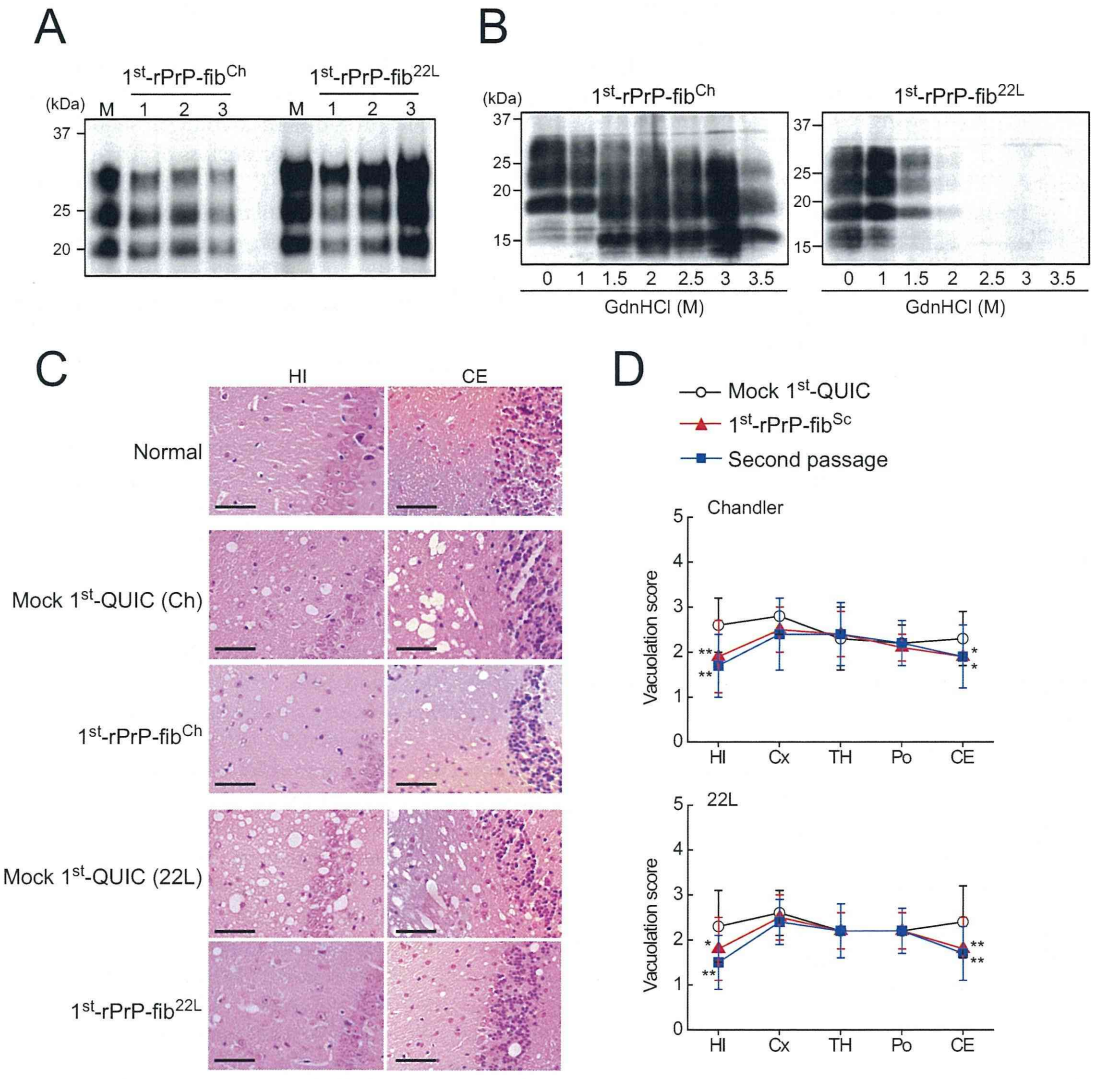

FIG 6 Bioassay of rPrP fibrils in mice. (A) PrP^{Sc} in the brains of prion-affected mice inoculated with 1st-rPrP-fib^{Ch} or 1st-rPrP-fib^{22L} was analyzed by Western blotting using anti-PrP antibody M20. Lanes M, mock 1st QUIC for strains Chandler and 22L. (B) The strain-specific properties of PrP^{Sc} in the brains of mice inoculated with 1st-rPrP-fib^{Sc} were examined by a conformational stability assay with GdnHCl (0 to 3.5 M). (C) Sections of the hippocampus (HI) and cerebellum (CE), stained with hematoxylin-eosin, from healthy mice, mice inoculated with 1st-rPrP-fib^{Sc}, and mock 1st QUIC-inoculated mice at terminal stages are shown. Bars, 50 μm. (D) Lesion profiles of spongiform changes in the hippocampus, cerebral cortex (Cx), thalamus (TH), pons (Po), and cerebellum were compared. Data are expressed as means ± SDs ($n = 3$). Statistical significance was determined using Mann-Whitney's U test. **, $P < 0.01$; *, $P < 0.05$.

generated at pH 4 in the first round were similar to those seen for 5th-rPrP-fib^{Sc} (Fig. 4B). These observations also support this hypothesis and suggest that the amplification of nonspecific rPrP fibrils is accelerated by certain conditions, such as an acidic environment. Further studies are needed to investigate whether unknown cofactors or environmental conditions are required to maintain the strain-specific conformations in subsequent rounds. On the other hand, this hypothesis also explains why prion infectivity was lost in the fifth round of RT-QUIC, as nonspecific rPrP fibrils generated during the serial RT-QUIC would be noninfectious. Although there remains the question as to what exactly the conformational differences between the noninfectious and infectious forms of rPrP fibrils are, the lack of cofactor molecules, such as SDS and synthetic PE, in the RT-QUIC might enhance the amplification of nonspecific rPrP fibrils lacking prion infectivity. Moreover, the fact that prion infectivity is sometimes too low to be detected and, more frequently, the fact that prion infectivity declines in the serial rPrP-PMCA (24, 25) or BH-PMCA (51–53) are consistent with the hypothesis.

ACKNOWLEDGMENTS

We thank Takashi Suematsu for help with the electron microscopy study and Matsuo Atsuko and Ayumi Yamakawa for technical assistance.

This work was supported by a grant-in-aid for young scientists (B; grant no. 21790846) from the Ministry of Education, Culture, Sports, Science and Technology of Japan, a grant for BSE research, and a grant-in-aid from the Research Committee of Prion Disease and Slow Virus Infection from the Ministry of Health, Labor and Welfare of Japan.

REFERENCES

1. **Prusiner SB.** 1991. Molecular biology of prion diseases. Science **252:** 1515–1522. http://dx.doi.org/10.1126/science.1675487.

2. **Weissmann C, Enari M, Klohn PC, Rossi D, Flechsig E.** 2002. Molecular biology of prions. Acta Neurobiol. Exp. (Wars.) **62**:153–166.
3. **Meyer RK, McKinley MP, Bowman KA, Braunfeld MB, Barry RA, Prusiner SB.** 1986. Separation and properties of cellular and scrapie prion proteins. Proc. Natl. Acad. Sci. U. S. A. **83**:2310–2314. http://dx.doi.org/10.1073/pnas.83.8.2310.
4. **Caughey BW, Dong A, Bhat KS, Ernst D, Hayes SF, Caughey WS.** 1991. Secondary structure analysis of the scrapie-associated protein PrP 27-30 in water by infrared spectroscopy. Biochemistry **30**:7672–7680. http://dx.doi.org/10.1021/bi00245a003.
5. **Pan KM, Baldwin M, Nguyen J, Gasset M, Serban A, Groth D, Mehlhorn I, Huang Z, Fletterick RJ, Cohen FE, Prusiner SB.** 1993. Conversion of alpha-helices into beta-sheets features in the formation of the scrapie prion proteins. Proc. Natl. Acad. Sci. U. S. A. **90**:10962–10966. http://dx.doi.org/10.1073/pnas.90.23.10962.
6. **Caughey B, Raymond GJ, Bessen RA.** 1998. Strain-dependent differences in beta-sheet conformations of abnormal prion protein. J. Biol. Chem. **273**:32230–32235. http://dx.doi.org/10.1074/jbc.273.48.32230.
7. **Atarashi R, Sim VL, Nishida N, Caughey B, Katamine S.** 2006. Prion strain-dependent differences in conversion of mutant prion proteins in cell culture. J. Virol. **80**:7854–7862. http://dx.doi.org/10.1128/JVI.00424-06.
8. **Thomzig A, Spassov S, Friedrich M, Naumann D, Beekes M.** 2004. Discriminating scrapie and bovine spongiform encephalopathy isolates by infrared spectroscopy of pathological prion protein. J. Biol. Chem. **279**:33847–33854. http://dx.doi.org/10.1074/jbc.M403730200.
9. **Baron GS, Hughson AG, Raymond GJ, Offerdahl DK, Barton KA, Raymond LD, Dorward DW, Caughey B.** 2011. Effect of glycans and the glycophosphatidylinositol anchor on strain dependent conformations of scrapie prion protein: improved purifications and infrared spectra. Biochemistry **50**:4479–4490. http://dx.doi.org/10.1021/bi2003907.
10. **Peretz D, Scott MR, Groth D, Williamson RA, Burton DR, Cohen FE, Prusiner SB.** 2001. Strain-specified relative conformational stability of the scrapie prion protein. Protein Sci. **10**:854–863. http://dx.doi.org/10.1110/ps.39201.
11. **Shindoh R, Kim CL, Song CH, Hasebe R, Horiuchi M.** 2009. The region approximately between amino acids 81 and 137 of proteinase K-resistant PrPSc is critical for the infectivity of the Chandler prion strain. J. Virol. **83**:3852–3860. http://dx.doi.org/10.1128/JVI.01740-08.
12. **Saborio GP, Permanne B, Soto C.** 2001. Sensitive detection of pathological prion protein by cyclic amplification of protein misfolding. Nature **411**:810–813. http://dx.doi.org/10.1038/35081095.
13. **Castilla J, Saa P, Hetz C, Soto C.** 2005. In vitro generation of infectious scrapie prions. Cell **121**:195–206. http://dx.doi.org/10.1016/j.cell.2005.02.011.
14. **Castilla J, Morales R, Saa P, Barria M, Gambetti P, Soto C.** 2008. Cell-free propagation of prion strains. EMBO J. **27**:2557–2566. http://dx.doi.org/10.1038/emboj.2008.181.
15. **Deleault NR, Harris BT, Rees JR, Supattapone S.** 2007. Formation of native prions from minimal components in vitro. Proc. Natl. Acad. Sci. U. S. A. **104**:9741–9746. http://dx.doi.org/10.1073/pnas.0702662104.
16. **Imamura M, Kato N, Yoshioka M, Okada H, Iwamaru Y, Shimizu Y, Mohri S, Yokoyama T, Murayama Y.** 2011. Glycosylphosphatidylinositol anchor-dependent stimulation pathway required for generation of baculovirus-derived recombinant scrapie prion protein. J. Virol. **85**:2582–2588. http://dx.doi.org/10.1128/JVI.02098-10.
17. **Imamura M, Kato N, Okada H, Yoshioka M, Iwamaru Y, Shimizu Y, Mohri S, Yokoyama T, Murayama Y.** 2013. Insect cell-derived cofactors become fully functional after proteinase K and heat treatment for high-fidelity amplification of glycosylphosphatidylinositol-anchored recombinant scrapie and BSE prion proteins. PLoS One **8**:e82538. http://dx.doi.org/10.1371/journal.pone.0082538.
18. **Legname G, Baskakov IV, Nguyen HO, Riesner D, Cohen FE, DeArmond SJ, Prusiner SB.** 2004. Synthetic mammalian prions. Science **305**:673–676. http://dx.doi.org/10.1126/science.1100195.
19. **Colby DW, Giles K, Legname G, Wille H, Baskakov IV, DeArmond SJ, Prusiner SB.** 2009. Design and construction of diverse mammalian prion strains. Proc. Natl. Acad. Sci. U. S. A. **106**:20417–20422. http://dx.doi.org/10.1073/pnas.0910350106.
20. **Raymond GJ, Race B, Hollister JR, Offerdahl DK, Moore RA, Kodali R, Raymond LD, Hughson AG, Rosenke R, Long D, Dorward DW, Baron GS.** 2012. Isolation of novel synthetic prion strains by amplification in transgenic mice coexpressing wild-type and anchorless prion proteins. J. Virol. **86**:11763–11778. http://dx.doi.org/10.1128/JVI.01353-12.
21. **Makarava N, Kovacs GG, Bocharova O, Savtchenko R, Alexeeva I, Budka H, Rohwer RG, Baskakov IV.** 2010. Recombinant prion protein induces a new transmissible prion disease in wild-type animals. Acta Neuropathol. **119**:177–187. http://dx.doi.org/10.1007/s00401-009-0633-x.
22. **Wang F, Wang X, Yuan CG, Ma J.** 2010. Generating a prion with bacterially expressed recombinant prion protein. Science **327**:1132–1135. http://dx.doi.org/10.1126/science.1183748.
23. **Zhang Z, Zhang Y, Wang F, Wang X, Xu Y, Yang H, Yu G, Yuan C, Ma J.** 2013. De novo generation of infectious prions with bacterially expressed recombinant prion protein. FASEB J. **27**:4768–4775. http://dx.doi.org/10.1096/fj.13-233965.
24. **Timmes AG, Moore RA, Fischer ER, Priola SA.** 2013. Recombinant prion protein refolded with lipid and RNA has the biochemical hallmarks of a prion but lacks in vivo infectivity. PLoS One **8**:e71081. http://dx.doi.org/10.1371/journal.pone.0071081.
25. **Kim JI, Cali I, Surewicz K, Kong Q, Raymond GJ, Atarashi R, Race B, Qing L, Gambetti P, Caughey B, Surewicz WK.** 2010. Mammalian prions generated from bacterially expressed prion protein in the absence of any mammalian cofactors. J. Biol. Chem. **285**:14083–14087. http://dx.doi.org/10.1074/jbc.C110.113464.
26. **Deleault NR, Piro JR, Walsh DJ, Wang F, Ma J, Geoghegan JC, Supattapone S.** 2012. Isolation of phosphatidylethanolamine as a solitary cofactor for prion formation in the absence of nucleic acids. Proc. Natl. Acad. Sci. U. S. A. **109**:8546–8551. http://dx.doi.org/10.1073/pnas.1204498109.
27. **Deleault NR, Walsh DJ, Piro JR, Wang F, Wang X, Ma J, Rees JR, Supattapone S.** 2012. Cofactor molecules maintain infectious conformation and restrict strain properties in purified prions. Proc. Natl. Acad. Sci. U. S. A. **109**:E1938–E1946. http://dx.doi.org/10.1073/pnas.1206999109.
28. **Atarashi R, Satoh K, Sano K, Fuse T, Yamaguchi N, Ishibashi D, Matsubara T, Nakagaki T, Yamanaka H, Shirabe S, Yamada M, Mizusawa H, Kitamoto T, Klug G, McGlade A, Collins SJ, Nishida N.** 2011. Ultrasensitive human prion detection in cerebrospinal fluid by real-time quaking-induced conversion. Nat. Med. **17**:175–178. http://dx.doi.org/10.1038/nm.2294.
29. **Wilham JM, Orru CD, Bessen RA, Atarashi R, Sano K, Race B, Meade-White KD, Taubner LM, Timmes A, Caughey B.** 2010. Rapid end-point quantitation of prion seeding activity with sensitivity comparable to bioassays. PLoS Pathog. **6**:e1001217. http://dx.doi.org/10.1371/journal.ppat.1001217.
30. **Atarashi R, Moore RA, Sim VL, Hughson AG, Dorward DW, Onwubiko HA, Priola SA, Caughey B.** 2007. Ultrasensitive detection of scrapie prion protein using seeded conversion of recombinant prion protein. Nat. Methods **4**:645–650. http://dx.doi.org/10.1038/nmeth1066.
31. **Fujihara A, Atarashi R, Fuse T, Ubagai K, Nakagaki T, Yamaguchi N, Ishibashi D, Katamine S, Nishida N.** 2009. Hyperefficient PrP Sc amplification of mouse-adapted BSE and scrapie strain by protein misfolding cyclic amplification technique. FEBS J. **276**:2841–2848. http://dx.doi.org/10.1111/j.1742-4658.2009.07007.x.
32. **Kocisko DA, Lansbury PT, Jr, Caughey B.** 1996. Partial unfolding and refolding of scrapie-associated prion protein: evidence for a critical 16-kDa C-terminal domain. Biochemistry **35**:13434–13442. http://dx.doi.org/10.1021/bi9610562.
33. **Atarashi R, Sano K, Satoh K, Nishida N.** 2011. Real-time quaking-induced conversion: a highly sensitive assay for prion detection. Prion **5**:150–153. http://dx.doi.org/10.4161/pri.5.3.16893.
34. **Smirnovas V, Baron GS, Offerdahl DK, Raymond GJ, Caughey B, Surewicz WK.** 2011. Structural organization of brain-derived mammalian prions examined by hydrogen-deuterium exchange. Nat. Struct. Mol. Biol. **18**:504–506. http://dx.doi.org/10.1038/nsmb.2035.
35. **McGuire LI, Peden AH, Orru CD, Wilham JM, Appleford NE, Mallinson G, Andrews M, Head MW, Caughey B, Will RG, Knight RS, Green AJ.** 2012. Real time quaking-induced conversion analysis of cerebrospinal fluid in sporadic Creutzfeldt-Jakob disease. Ann. Neurol. **72**:278–285. http://dx.doi.org/10.1002/ana.23589.
36. **Orru CD, Wilham JM, Raymond LD, Kuhn F, Schroeder B, Raeber AJ, Caughey B.** 2011. Prion disease blood test using immunoprecipitation and improved quaking-induced conversion. mBio **2**(3):e00078-00011. http://dx.doi.org/10.1128/mBio.00078-11.
37. **Sano K, Satoh K, Atarashi R, Takashima H, Iwasaki Y, Yoshida M, Sanjo N, Murai H, Mizusawa H, Schmitz M, Zerr I, Kim YS, Nishida N.**

2013. Early detection of abnormal prion protein in genetic human prion diseases now possible using real-time QUIC assay. PLoS One **8**:e54915. http://dx.doi.org/10.1371/journal.pone.0054915.

38. **Vascellari S, Orru CD, Hughson AG, King D, Barron R, Wilham JM, Baron GS, Race B, Pani A, Caughey B.** 2012. Prion seeding activities of mouse scrapie strains with divergent PrPSc protease sensitivities and amyloid plaque content using RT-QuIC and eQuIC. PLoS One **7**:e48969. http://dx.doi.org/10.1371/journal.pone.0048969.
39. **Henderson DM, Manca M, Haley NJ, Denkers ND, Nalls AV, Mathiason CK, Caughey B, Hoover EA.** 2013. Rapid antemortem detection of CWD prions in deer saliva. PLoS One **8**:e74377. http://dx.doi.org/10.1371/journal.pone.0074377.
40. **Smirnovas V, Kim JI, Lu X, Atarashi R, Caughey B, Surewicz WK.** 2009. Distinct structures of scrapie prion protein (PrPSc)-seeded versus spontaneous recombinant prion protein fibrils revealed by hydrogen/deuterium exchange. J. Biol. Chem. **284**:24233–24241. http://dx.doi.org/10.1074/jbc.M109.036558.
41. **Hornemann S, Schorn C, Wuthrich K.** 2004. NMR structure of the bovine prion protein isolated from healthy calf brains. EMBO Rep. **5**:1159–1164. http://dx.doi.org/10.1038/sj.embor.7400297.
42. **Clarke AR, Jackson GS, Collinge J.** 2001. The molecular biology of prion propagation. Philos. Trans. R. Soc. Lond. B Biol. Sci. **356**:185–195. http://dx.doi.org/10.1098/rstb.2000.0764.
43. **Lawson VA, Collins SJ, Masters CL, Hill AF.** 2005. Prion protein glycosylation. J. Neurochem. **93**:793–801. http://dx.doi.org/10.1111/j.1471-4159.2005.03104.x.
44. **Aguzzi A, Heikenwalder M, Polymenidou M.** 2007. Insights into prion strains and neurotoxicity. Nat. Rev. Mol. Cell Biol. **8**:552–561. http://dx.doi.org/10.1038/nrm2204.
45. **Cancellotti E, Mahal SP, Somerville R, Diack A, Brown D, Piccardo P, Weissmann C, Manson JC.** 2013. Post-translational changes to PrP alter transmissible spongiform encephalopathy strain properties. EMBO J. **32**:756–769. http://dx.doi.org/10.1038/emboj.2013.6.
46. **Piro JR, Harris BT, Nishina K, Soto C, Morales R, Rees JR, Supattapone S.** 2009. Prion protein glycosylation is not required for strain-specific neurotropism. J. Virol. **83**:5321–5328. http://dx.doi.org/10.1128/JVI.02502-08.
47. **Mahal SP, Jablonski J, Suponitsky-Kroyter I, Oelschlegel AM, Herva ME, Oldstone M, Weissmann C.** 2012. Propagation of RML prions in mice expressing PrP devoid of GPI anchor leads to formation of a novel, stable prion strain. PLoS Pathog. **8**:e1002746. http://dx.doi.org/10.1371/journal.ppat.1002746.
48. **Li J, Browning S, Mahal SP, Oelschlegel AM, Weissmann C.** 2010. Darwinian evolution of prions in cell culture. Science **327**:869–872. http://dx.doi.org/10.1126/science.1183218.
49. **Weissmann C, Li J, Mahal SP, Browning S.** 2011. Prions on the move. EMBO Rep. **12**:1109–1117. http://dx.doi.org/10.1038/embor.2011.192.
50. **Shikiya RA, Ayers JI, Schutt CR, Kincaid AE, Bartz JC.** 2010. Coinfecting prion strains compete for a limiting cellular resource. J. Virol. **84**:5706–5714. http://dx.doi.org/10.1128/JVI.00243-10.
51. **Bieschke J, Weber P, Sarafoff N, Beekes M, Giese A, Kretzschmar H.** 2004. Autocatalytic self-propagation of misfolded prion protein. Proc. Natl. Acad. Sci. U. S. A. **101**:12207–12211. http://dx.doi.org/10.1073/pnas.0404650101.
52. **Klingeborn M, Race B, Meade-White KD, Chesebro B.** 2011. Lower specific infectivity of protease-resistant prion protein generated in cell-free reactions. Proc. Natl. Acad. Sci. U. S. A. **108**:E1244–E1253. http://dx.doi.org/10.1073/pnas.1111255108.
53. **Gonzalez-Montalban N, Lee YJ, Makarava N, Savtchenko R, Baskakov IV.** 2013. Changes in prion replication environment cause prion strain mutation. FASEB J. **27**:3702–3710. http://dx.doi.org/10.1096/fj.13-230466.

Dementia Japan 28：189-196, 2014

特集　1. 認知症診療最前線

プリオン病の新しい診断法

佐藤　克也，新　竜一郎，西田　教行

1. はじめに

近年認知症を呈する疾患の疾患概念・診断基準が急速に確立し，さらに認知症を呈する神経変性疾患群や自己免疫性脳症などの臨床診断の精度も徐々に向上している．一般的な認知症疾患は，認知機能障害を思わせる症状に気づいてから認知症として寝たきりになるまでに8-10年を要する．

しかしながらプリオン病を含めた急速進行性認知症は，認知機能障害が約1-2年以内に急速に進行し，約3年以内に寝たきりになる．急速進行性認知症の中には治療可能な疾患群も含まれており，血液・髄液検査・画像検査の重要性も高まっている．

今回ヒトプリオン病の髄液中の新しい診断法について詳述する．

New diagnostic method, "Real-time qucking-induced conversion (RT-QuIC) method", in CSF analysis of patients with prion disease
Katsuya Satoh, Ryuichiro Atarashi, Noriyuki Nishida
長崎大学医歯薬学総合研究科感染分子解析学分野［〒852-8523 長崎県長崎市坂本1-12-4　基礎棟8F］
Department of Molecular Microbiology and Immunology, Nagasaki University Graduate School of Biomedical Sciences (1-12-4 Sakamoto, Nagasaki 852-8501, Japan)

2. 現在のプリオン病の診断基準（表1）(Brandel et al., 2000)

プリオン病における髄液診断は1996年Hsichらが髄液中の14-3-3蛋白の有効性を示し（Hsich et al., 1996），1998年WHO診断基準の補助項目の一つとなったために，プリオン病における髄液検査が重要視されるようになった（Brandel et al., 2000）（表1）．さらにバイオマーカーとして総タウ蛋白の発見以後，プリオン病における髄液検査がさらに重要視されている．しかしながら孤発性プリオン病の早期診断では髄液中の14-3-3蛋白や総タウ蛋白の検出感度は低い（Satoh et al., 2007）．

一方孤発性プリオン病は1999年Parchiの報告（Parchi et al., 1999）ではプリオン病患者の脳組織・病理像とプリオン蛋白遺伝子コドン129の多型に基づくと6つのサブタイプに分類されると言われている（表2）．この6つのサブタイプの中で，日本で比較的多いと考えられているMM2-皮質型とMM2-視床型の2つタイプはWHO診断基準を満たさない．さらに髄液中の14-3-3蛋白や総タウ蛋白の陽性率が低い．そのためプリオン病の髄液中の既存のバイオマーカー以外の特異度の高い検査が必要になっている．

さらにMM2-皮質型とMM2-視床型は，急速進行

表1. WHO診断基準

1. 進行性認知機能障害
2. A ミオクローヌス
   B 視覚異常又は小脳失調
   C 錐体路障害又は錐体外路障害
   D 無動性無言
3. A 脳波上PSD
   B 髄液14-3-3蛋白陽性で全臨床経過が2年未満であるもの.

possible CJD：ほぼ確実例と同様の臨床症状を呈するが，脳波上の周期性同期性放電を認めないもの．具体的には最大2年の期間で1及び2で2項目以上陽性を示す．
probable CJD：病理所見・異常プリオン蛋白の証明は得られていないが，進行性認知症を示し，さらに脳波上の周期性同期性放電を認める．具体的には
1及び2で2項目以上陽性を示し，3で1項目以上陽性を示すこと，又は「3. 疑い例」に該当する例で，特に3で2の項目で全臨床経過が2年未満であるもの．
definite CJD：脳組織においてCJDに特徴的な病理所見を証明するか，またはウェスタンブロット法か免疫組織学的検査にて異常プリオン蛋白が検出されたもの．孤発性CJDに一致した病理像を持つこと．

性認知症との鑑別が極めて重要であり，画像診断以外の方法が重要である（MM2-視床型は特徴的なMR拡散強調画像の所見を示さないことが多い）．そのため特異度の高い検査，つまりプリオン病の原因物質である異常プリオン蛋白の検出を，髄液を含めたヒト生体材料から検出する事が必要になっている．

3. プリオン病と鑑別すべき急速進行性認知症とは？

上述したように孤発性プリオン病のMM2-皮質型とMM2-視床型は急速に認知機能障害が進行する急速進行性認知症と鑑別する必要性がある．

急速進行性認知症はカルフォルニア大学サンフランシスコ校のGeschwindが2008年に提唱した概念であり，最初の報告では急速に認知症を来した179症例について検討を行っている（Geschwind et al., 2008）．その179症例中で，プリオン病患者は62%，非プリオン病は38%を示していた．非プリオン病患者の中で約39%は神経変性疾患で，22%は自己免疫関連性脳症で，6%は悪性疾患・感染症であった．

その後JosephsはMayo Clinicを受診し認知機能障害を呈し剖検になった神経変性疾患の中で，罹病期間が4年以内の症例であった22症例について検討を行った（Josephs et al., 2009）．約36%はクロイツフェルト・ヤコブ病（Creutzfeldt-Jakob disease：孤発性プリオン病）であったが，frontal temporal lobular dementia with motor neuron disease（TDP-43 proteinopathy）が約23%，tauopathyが約9%であった．

Stoeckらが急速進行性認知症について約10年間（1998年-2007年）の追跡調査した10,731症例の検討では，プリオン病では約35%，神経変性疾患は28%，炎症性疾患は約7%，傍腫瘍症候群は約3%，

表2. 孤発性プリオン病の分類

遺伝子型：蛋白型	MM1	MM2	MM2	MV1	MV2	VV1	VV2
病型	典型的CJD	皮質型	/視床型	典型的CJD	失調・認知症型	認知症型	失調・認知症型
プリオン蛋白の沈着パターン	シナプス型	シナプス型	シナプス型	シナプス型	シナプス型 プラーク型	シナプス型	シナプス型 プラーク型
ミオクローヌス	+	−	−	+	+	−	+
周期性同期性放電	+	−	−	+	まれ	−	まれ
14-3-3蛋白	+	÷	—	+	まれ	+	+
進行速度	亜急性	緩徐	緩徐	亜急性	緩徐	緩徐	亜急性

脳血管関連疾患は約5%であった（Stoeck et al., 2012）．神経変性疾患の中では，アルツハイマー型認知症が37%，脳血管性認知症が7%，レビー小体型認知症が14.4%，前頭側頭型皮質変性症が約6%であった．

上記の研究・検討結果により急速進行性認知症を来す疾患でプリオン病と鑑別すべき疾患は，アルツハイマー型認知症や前頭側頭葉変性性認知症などの神経変性疾患，橋本脳症を含めた自己免疫関連性脳症，limbic encephalitis などの傍腫瘍症候群や血管内悪性リンパ腫・glioblastoma などの悪性疾患，感染症等などである．

又橋本脳症，limbic encephalitis などの傍腫瘍症候群，低酸素脳症，痙攣後脳症などはMR拡散強調画像にて大脳皮質が高信号を示し，急速な認知機能障害を呈する．これらの疾患は髄液中の既存のバイオマーカーとではプリオン病との鑑別が極めて難しい．そのため特異度の高い検査，つまり孤発性プリオン病の原因物質である異常プリオン蛋白の検出を，髄液を含めたヒト生体材料から検出する事が必要になっている．

4. 既存の髄液中のバイオマーカーとは？

4.1 14-3-3 蛋白

14-3-3 蛋白は Hsich らが孤発性プリオン病患者の中で孤発性孤発性プリオン病患者と正常人の脳組織を二次元電気泳動で比較・検討し，14-3-3 蛋白を同定し，孤発性プリオン病患者での脳組織・脳脊髄液での特異性を示した（Hsich et al., 1996）．同年 Zerr らが孤発性プリオン病患者の脳脊髄液を Hsich と同様な方法で解析し 14-3-3 蛋白を同定し，脳脊髄液中での 14-3-3 蛋白の有用性を示した（Zerr et al., 1996）．Zerr らはプリオン病患者 289 症例について検討を行っている（Zerr et al., 1998）．最初の Hsich らの報告では感度 96%，特異度は 99% であったが，その後 Zerr らの報告では，孤発性プリオン病患者においては 173 症例中 155 症例（89.5%）で陽性を示した（Zerr et al., 1998）．

14-3-3 蛋白はウェスタンブロットで解析を行うため，抗体（一次抗体や二次抗体）や使っているキットなどが違うために他国と比較は難しい．そのためドイツの Zerr らが中心となり，14-3-3 蛋白の検査の標準化が開始されている．

Stoeck らが急速進行性認知症患者における 14-3-3 蛋白陽性の神経疾患・神経変性疾患を示す疾患・感度について検討されている（Stoeck et al., 2012）．

4.2 総タウ蛋白

1998 年 WHO の診断基準の拡大診断基準では，髄液検査では 14-3-3 蛋白が補助的診断基準項目の一つとして加えられている．日本とヨーロッパ孤発性プリオン病サーベイランスグループは，孤発性プリオン病患者の髄液中の 14-3-3 蛋白と総タウ蛋白が診断に有効であると報告した．

一方 1997 年 Otto らは脳脊髄液中の総タウ蛋白の異常高値を報告し（Otto et al., 1997），さらに 2002 年に Otto らは 297 人の孤発性プリオン病患者の脳脊髄液の 14-3-3 蛋白と総タウ蛋白の比較検討を行った（Otto et al., 2002）．これらの報告では総タウ蛋白が感度 94%・特異度 90% であることを示し，14-3-3 蛋白より特異度・感度において優れていることを確認した．

Stoeck らが急速進行性認知症患者における総タウ蛋白（>1,300 pg/ml）陽性の神経疾患・神経変性疾患を示す疾患・感度について検討されている（Stoeck et al., 2012）．

我々 2004 年急速進行性認知症の中で非典型的なアルツハイマー型認知症があり，総タウ蛋白が >1,160 pg/ml を超えるような急速進行性アルツハイマー型認知症が存在する．そのため孤発性プリオン病と急速進行性アルツハイマー型認知症と鑑別が必要であると考え，リン酸化タウ蛋白と総タウ蛋白の比で鑑別することが可能であることを示した（Satoh et al., 2006）．

現在海外との診断値をあせわるために総タウ蛋白のカットオフ地を（>1,300 pg/ml）陽性とした．

以上により孤発性プリオン病患者の髄液中の総タウ蛋白が診断に有効であるが，急速進行性アルツハイマー型認知症ではリン酸化タウ蛋白と総タウ蛋白

の比で鑑別することが可能である.

4.3 まとめ

2010年以降イギリス（Otto et al., 2002）やカナダ（Stoeck et al., 2012）を含めた多くの国々でプリオン病患者における髄液中のバイオマーカー前向き研究を行われ，感度・特異度が再報告されてきた．これらの結果では感度・特異度は70-80%程度であった．これらの論文でも髄液中の14-3-3蛋白偽陽性と総タウ蛋白（1,300 pg/ml）偽陽性を示す疾患を挙げ，鑑別することの重要性を示した．しかしながらこの論文を含めて孤発性プリオン病の診断バイオマーカーの研究にはいろいろな問題を含んでいる．特に診断バイオマーカーで利用される14-3-3蛋白や総タウ蛋白は研究者間で全く異なる．現在各国間の比較ができるように標準化の試みが2012年より開始された．現在髄液中の14-3-3蛋白の測定のための抗体や総タウ蛋白を測定できうるELISAキットまで詳細に決める事となり，カットオフ値を行うことになった.

5. Real-time qucking-induced conversion（RT-QuIC）法による異常プリオン蛋白の検出

急速進行性認知症の中でプリオン病特異的な方法を用いて，解析することが決めて重要であり，必要性が高まってきた.

プリオン病を引き起こす感染病原体は，プリオン（PrP）と呼ばれ，プリオンはおそらくは単一のタンパク質である異常型PrPのみから構成されている，とするタンパク単独仮説が提唱され，それを支持する多くの実験結果の集積と共に，その仮説が受け入れられるようになっている（Satoh et al., 2006）.

異常型PrPは，正常型PrPが構造上変化したもので，外部より異常型PrPが宿主細胞内に侵入すると，細胞内で恒常的に発現する正常型PrPに作用し，正常型PrPから異常型PrPへの構造変化が誘導される．異常型PrPと正常型PrPではアミノ酸配列に違いはなく，その立体構造のみが異なっている．正常型PrPはα-helix構造を多く含み，可溶性で柔軟な構造をしているが，異常型PrPはβ-sheet含量が非常に高く，そのため凝集しやすく不溶性，蛋白分解酵素処理に抵抗性などの性質を持つ．しかし，正常型PrPから異常型PrPへの構造変換プロセスがプリオン病の本質であると考えられている．異常型PrPは，主に神経系に発現している正常型PrPが構造上変化したもので，外部より異常型PrPが宿主細胞内に侵入すると，細胞内で恒常的に発現する正常型PrPに作用し，正常型PrPから異常型PrPへの構造変化が誘導される．異常型PrPと正常型PrPではアミノ酸配列に違いが，その立体構造のみが異なっている．正常型PrPはα-helix構造を多く含み，可溶性で柔軟な構造をしているが，異常型PrPはβ-sheet含量が非常に高く，そのため凝集しやすく不溶性，蛋白分解酵素処理に抵抗性などの性質を持つ．正常型から異常型への変換が起こる原因として第一に，プリオン感染組織等の汚染により，外部から生体内に侵入した異常型が正常型を次々に自分自身と同じ構造に変換するというメカニズムが挙げられる．さらに生体内で正常型PrPが，異常型PrPへと変化し，それが変換反応の種となり，正常型から異常型への変換反応が進行するというものである.

近年正常PrPを反応基質として，試験管内で微量の異常型PrPを検出が容易なレベルまで増幅することが可能なことが報告され，それを用いた新たな診断法の開発が検討されてきた．しかしそれぞれの動物種やプリオン株により増幅効率が異なることもあり，孤発性プリオン病での高効率の増幅は達成されていなかった．一方，我々はQuIC法（Quaking-Induced Conversion）という，孤発性プリオン病に対して非常に感度の高い異常型PrP増幅法を開発することに成功し，これを用いた孤発性プリオン病髄液診断が可能であることを示した（Chohan et al., 2012）．現在我々が開発した異常型PrP高感度増幅法（Real-time QuIC法）はプリオン病のみでなく，神経変性疾患に応用できると思われる．我々は，最近異常型PrP高感度増幅法（Real-time QuIC法と命名）を開発し，ヒトプリオン病患者由来脳脊髄液中の異常型PrPを検出することに成功した．この方法は，異常型PrPを増幅反応の核（シード）とし

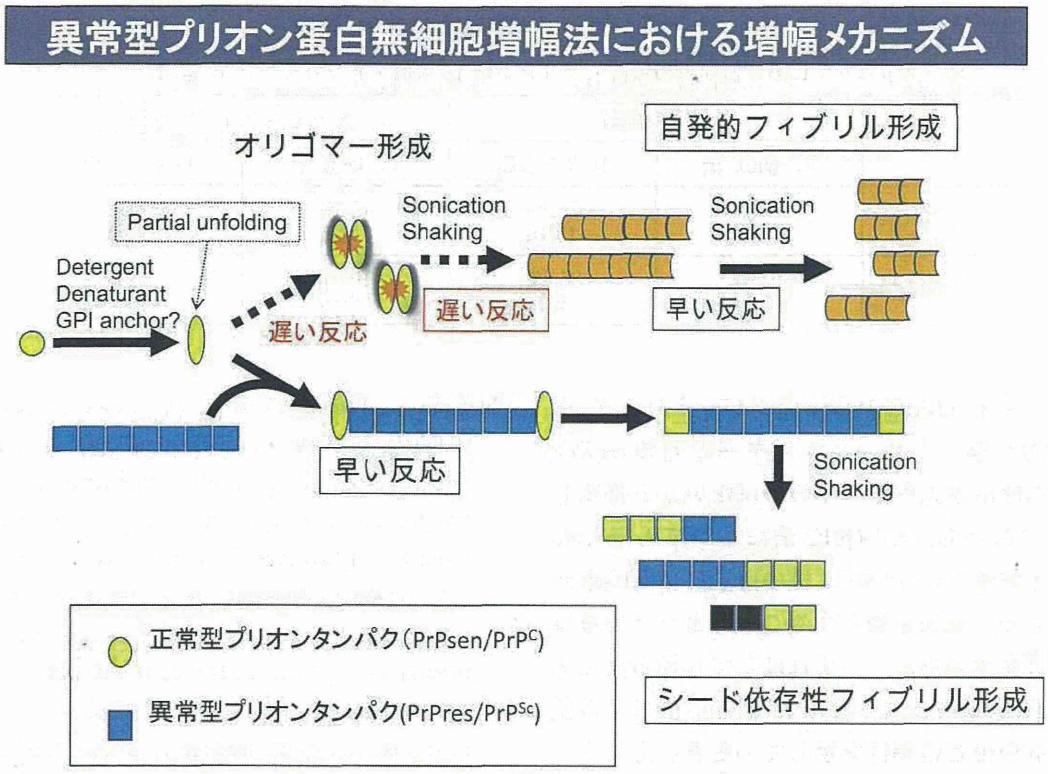

図 1.

て用いて，リコンビナント PrP（rPrP）の凝集（フィブリル形成）反応を連続的に試験管内で行わせ，サンプル（脳脊髄液）中の異常型 PrP を増幅して検出するという方式である（図 1 に増幅機構のモデルを示す）．感度を上げ，疑陽性反応をなくすためには，シード（異常型 PrP）依存的な反応は抑制せず，自然発生的なフィブリル形成反応のみ（spontaneous formation）を可能な限り抑制する条件を見出すことが必要であったが，成功し得た．

6. ヒトプリオン病患者の髄液検査への挑戦

われわれは RT-QuIC 法のプリオン病診断への有用性を検証するためにオーストラリアのメルボルン大学と共同研究として blind study を行った（Atarashi et al., 2011）．30 症例の磁液を無作為に送付してもらい，髄液生化学的マー力一測定と RT-QuIC 法を行った．測定終了後，オーストラリアに結果を送付し患者情報と照合した．その結果，プリオン病症例では i4/16（87.5%）で陽性となり，一方，非プリオン病症例では全て陸性（0/14）であった（表 3）．

2012 年にはイギリスの Green らのグループが RT-QuIC 法による髄液プリオン病診断の検討を行い，その結果を報告している（McGuire et al., 2012）．その論文によると，プリオン病症例では 109/123（88.6%）で陽性であり，非プリオン病症例では 1/103 で特異度は 99% であった．なお，偽陽性となった 1 例は脳血管性認知症の診断であったが，病理解剖はされておらず，2 人の独立した神経内科医による再調査ではプリオン病の可能性も否定できないと書かれている．Green らの基本的な RT-QuIC 法の実験手法（McGuire et al., 2012）はわれわれと共通であるが，異なる点としては，使用する recPrP はわれわれがヒト配列のものであるのに対してハムスター配列のものを用いていることと，蛍光プレートリーダーの機種が速うことがあげられる．われわれの使用している機極（テカン社製蛍光プレートリーダー）ではハムスター配列の recPrP を反応基質として RT-QuIC 法を行うと，ヒト配列の recPrP と比べ感度が明らかに低くなるが，おそらく彼女らの使

表3. RT-QuIC 法の髄液検査への応用
（日本における症例の検討：プリオン病18症例・非プリオン病35症例，bind study でのオーストラリアにおける症例の検討：プリオン病16症例・非プリオン病14症例）

	日本の症例		オーストラリアの症例	
	RT-QuIC 法	14-3-3 蛋白	RT-QuIC 法	14-3-3 蛋白
感度	83.3% 15/18	72.2% 13/18	87.5% 14/16	87.5% 14/16
特異度	100% 0/35	85.7% 5/35	100% 0/14	71.4% 4/14

用している機組（BMG 社製蛍光プレートリーダー）では撹拌力が強いため，ハムスター配列の recPrP でも十分な感度が達成できるのではないかと推測している．すなわち，RT-QuIC 法においても in vivo の場合ほど厳密ではないが「種の壁」に似た現象が観察されるが，撹拌を強くすることによりその壁は低くなる可能性がある．いずれにしても両者共に感度は 80〜90% であったことは RT-QuIC 法による髄液診断の有用性と信頼性を示しているといえよう．

文　献

Atarashi R, Satoh K, Sano K, et al. (2011) Ultrasensitive human prion detection in cerebrospinal fluid by real-time quaking-induced conversion. Nat Med 17(2): 175-178

Brandel JP, Delasnerie-Laupêtre N, Laplanche JL, Hauw JJ, Alpérovitch A (2000) Diagnosis of Creutzfeldt-Jakob disease : effect of clinical criteria on incidence estimates. Neurology 14 ; 54(5) : 1095-1099

Chohan G, et al. (2012) The role of cerebrospinal fluid 14-3-3 and other proteins in the diagnosis of sporadic CJD in the UK : a 10-year review. J Neurol Neurosurg Psychiatry 81 (11) : 1243-1248

Coulthart MB, et al. (2012) Diagnostic accuracy of cerebrospinal fluid protein markers for sporadic CJD in Canada : a 6-year prospective study. BMC Neurol 11 : 133

Geschwind MD, Shu H, Haman A, et al. (2008) Rapidly progressive dementia. Ann Neurol 64(1) : 97-108

Hsich G, Kenney K, Gibbs CJ, et al. (1996) The 14-3-3 brain protein in cerebrospinal fluid as a marker for transmissible spongiform encephalopathies. N Engl J Med 335 : 924-930

Josephs KA, Ahlskog JE, Parisi JE, Boeve BF, Crum BA, Giannini C, Petersen RC (2009) Rapidly progressive neurodegenerative dementias. Arch Neurol 66(2) : 201-207

McGuire LI, Peden AH, Orrú CD, Wilham JM, Appleford NE, Mallinson G, Andrews M, Head MW, Caughey B, Will RG, Knight RS, Green AJ (2012) Real time quaking-induced conversion analysis of cerebrospinal fluid in sporadic Creutzfeldt-Jakob disease. Ann Neurol 72(2) : 278-285

Otto M, Wiltfang J, Tumani H, et al. (1997) Elevated levels of tau-protein in cerebrospinal fluid of patients with Creutzfeldt-Jakob disease. Neurosci Lett 225 : 210-212

Otto M, Wiltfang J, Cepek L, et al. (2002) Tau protein and 14-3-3 protein in the differential diagnosis of Creutzfeldt-Jakob disease. Neurology 58 : 192-197

Parchi P, Giese A, Capellari S, Brown P, Schulz-Schaeffer W, Windl O, Zerr I, Budka H, Kopp N, Piccardo P, Poser S, Rojiani A, Streichemberger N, Julien J, Vital C, Ghetti B, Gambetti P, Kretzschmar H (1999) Classification of sporadic Creutzfeldt-Jakob disease based on molecular and phenotypic analysis of 300 subjects. Ann Neurol 46(2) : 224-233

Satoh K, Shirabe S, Eguchi H, et al. (2006) 14-3-3 protein, total tau and phosphorylated tau in Cerebrospinal fluid of patients with Creutzfeldt-Jakob disease and neurodegenerative disease in Japan. Cellular and molecular neurobiology 26 : 45-52

Satoh K, Shirabe S, Tsujino A, Eguchi H, Motomura M, Honda H, Tomita I, Satoh A, Tsujihata M, Matsuo H, Nakagawa M, Eguchi K (2007) Total tau protein in cerebrospinal fluid and diffusion-weighted MRI as an early diagnostic marker for Creutzfeldt-Jakob disease. Dement Geriatr Cogn Disord 24 (3) : 207-212

Stoeck K, Sanchez-Juan P, Gawinecka J, Green A, Ladogana A, Pocchiari M, Sanchez-Valle R, Mitrova E, Sklaviadis T, Kulczycki J, Slivarichova D, Saiz A, Calero M, Knight R, Aguzzi A, Laplanche JL, Peoc'h K, Schelzke G, Karch A, van Duijn CM, Zerr I (2012) Cerebrospinal fluid biomarker supported diagnosis of Creutzfeldt-Jakob disease and rapid dementias : a longitudinal multicentre study over 10 years. Brain 135

(Pt 10) : 3051-3061

Zerr I, Bodemer M, Otto M, et al. (1996) Diagnosis of Creutzfeldt-Jakob disease by two-dimensional gel electrophoresis of cerebrospinal fluid. Lancet 348 : 846-849

Zerr I, Bodemer M, Gefeller O, et al. (1998) Detection of 14-3-3 protein in the cerebrospinal fluid supports the diagnosis of Creutzfeldt-Jakob disease. Ann Neurol 43(1) : 32-40

Dementia Japan Vol. 28 No. 2 May 2014

New diagnostic method, "Real-time qucking-induced conversion (RT-QuIC) method", in CSF analysis of patients with prion disease

Katsuya Satoh, Ryuichiro Atarashi, Noriyuki Nishida

Department of Molecular Microbiology and Immunology, Nagasaki University Graduate School of Biomedical Sciences

Hsich et al. reported 14-3-3 protein in CSF supports a diagnosis of human prion disease, and 14-3-3 protein is one of supportive diagnostic criteria on WHO (1998). In the presence of 14-3-3 protein and total tau protein is widely used as a surrogate marker in the pre-mortem diagnosis of human prion disease and other rapidly progressive dementia. Most recent research report that the sensitivity of 14-3-3 protein was 43%-100%, and the specificity of 14-3-3 protein was 47%-97%. And the sensitivity of total tau protein was 43%-100%, and the specificity of total tau protein was 47%-97%. In other hand we recently developed a new in vitro amplification technology, designated "RT-QuIC assay", for the detection of PrP (Sc) in CSF of sCJD. Other group reported that CSF RT-QuIC method analysis has the potential to be a more specific diagnostic test for sCJD than current CSF tests, but their method is different from our method and their study was not enough. Now we are analyzing for the sensitivity and specificity of biomarkers and RT-QuIC method in CSF of definite cases of human prion disease, the number of definite cases of human prion disease is larger than that of other studies.

Address correspondence to Dr. Katsuya Satoh, Department of Molecular Microbiology and Immunology, Nagasaki University Graduate School of Biomedical Sciences (1-12-4 Sakamoto, Nagasaki 852-8501, Japan)

Dynein dysfunction disrupts β-amyloid clearance in astrocytes through endocytic disturbances

Nobuyuki Kimura[a,b], Sachi Okabayashi[b,c] and Fumiko Ono[b,c]

We showed previously that aging attenuates the interaction between dynein–dynactin complexes in cynomolgus monkey brain and that dynein dysfunction reproduces age-dependent endocytic disturbances, resulting in intracellular β-amyloid (Aβ) accumulation, synaptic vesicle transport deficits, and neuritic swelling. It remains unclear whether such endocytic disturbances also occur in glial cells. Here, we show that endocytic pathology, such as intracellular accumulation of enlarged endosomes, occurs in astrocytes of aged monkey brains. Also, Aβ accumulates in these enlarged endosomes. RNA interference studies have shown that dynein dysfunction reproduces astroglial endocytic pathology and disrupts Aβ clearance in astrocytes through endocytic disturbances. These findings suggest that endocytic disturbances can alter astroglial functions and may also be involved in age-dependent Aβ pathology. *NeuroReport* **25:514–520 © 2014 Wolters Kluwer Health | Lippincott Williams & Wilkins.**

NeuroReport 2014, 25:514–520

Keywords: aging, Alzheimer's disease, β-amyloid protein, astrocytes, dynein, endocytosis

[a]Section of Cell Biology and Pathology, Department of Alzheimer's Disease Research, Center for Development of Advanced Medicine for Dementia, National Center for Geriatrics and Gerontology, Aichi, [b]Tsukuba Primate Research Center, National Institute of Biomedical Innovation and [c]The Corporation for Production and Research of Laboratory Primates, Tsukuba, Japan

Correspondence to Nobuyuki Kimura, PhD, DVM, Section of Cell Biology and Pathology, Department of Alzheimer's Disease Research, Center for Development of Advanced Medicine for Dementia, National Center for Geriatrics and Gerontology, Gengo 35, Morioka, Obu, Aichi 474-8511, Japan
Tel: +81 562 44 5651 x6404; fax: +81 562 46 8569;
e-mail: kimura@ncgg.go.jp

Received 5 December 2013 **accepted** 8 January 2014

Introduction

Increasing evidence suggests that endocytic disturbances are involved in the pathogenesis of Alzheimer's disease (AD) [1–3]. We have reported previously that aging attenuates interactions between dynein and dynactin, the functional complex required for dynein-mediated transport in cynomolgus monkey brains [4]. We also showed that dynein dysfunction induces endocytic disturbances, resulting in the accumulation of intracellular β-amyloid (Aβ) protein, synaptic vesicle transport deficits, and neuritic swelling [5,6]. Thus, dynein dysfunction could be a causative factor in age-related endocytic disturbances, leading to AD pathogenesis.

Astrocytes are the most abundant glial cell type in the brain. Several studies suggest that astrocytes are also involved in the pathogenesis of AD, such as mediating Aβ clearance [7,8]. However, it remains unclear whether aging, independent of neurodegenerative disease, affects astroglial functions.

In aged cynomolgus monkey brains, we documented the spontaneous formation of senile plaques (SPs) and neurofibrillary tangles, both of which represent the major pathological features of AD brains [9,10]. The observation that the amino acid sequence of cynomolgus monkey Aβ is completely homologous to human Aβ [11] supports the idea that cynomolgus monkeys represent a good surrogate model for investigating age-related Aβ pathology.

In the present study, we investigated age-related changes in astrocytes by using cynomolgus monkey brains. Here, we show that endocytic pathology, such as intracellular accumulation of enlarged endosomes, occurs even in astrocytes of aged monkey brains. Immunohistochemical analyses also showed that affected astrocytes were located near sites of cerebral amyloid angiopathy (CAA). Moreover, RNA interference studies showed that dynein dysfunction reproduced endocytic pathology in cultured cynomolgus monkey astrocytes and disturbed Aβ clearance in astrocytes through endocytic disturbances.

Materials and methods

Animals

The temporal lobes of 12 cynomolgus monkeys (*Macaca fascicularis*) were used for immunohistochemical analyses. Of these, six brains were from young monkeys aged 4 ($N=4$) and 6 ($N=2$) years, and six were from aged monkeys aged 26 ($N=2$), 30, 32, and 36 ($N=2$) years. All brains were obtained from the Tsukuba Primate Research Center, National Institute of Biomedical Innovation, Ibaraki, Japan.

For astrocyte culture studies, embryonic day 18 Sprague–Dawley rats (SLC Japan, Shizuoka, Japan) and embryonic day 80 cynomolgus monkeys were used. The embryonic cynomolgus monkeys were also obtained from the Tsukuba Primate Research Center. All animal experiments were conducted according to the National Institute of Biomedical Innovation rules and guidelines for experimental animal welfare.

Immunohistochemistry

Brain samples were immersion fixed in 4% paraformaldehyde, embedded in paraffin, and cut into 4-μm-thick

0959-4965 © 2014 Wolters Kluwer Health | Lippincott Williams & Wilkins DOI: 10.1097/WNR.0000000000000124

sections. Sections were deparaffinized by pretreating with 0.5% periodic acid and then incubated with rabbit polyclonal anti-EEA1 antibody (Santa Cruz Biotechnology, Santa Cruz, California, USA) overnight at 4°C. Following brief washes, the sections were incubated sequentially with biotinylated goat anti-rabbit IgG, followed by streptavidin–biotin–horseradish peroxidase complex (Vector, Burlingame, California, USA). Immunoreactive elements were visualized by treating the sections with 3-3′ diaminobenzidine tetroxide (Dojin Kagaku, Kumamoto, Japan). The sections were then counterstained with hematoxylin.

For double and triple immunohistochemistry, sections were prestained with 1% Sudan Black B to reduce autofluorescence. Sections were incubated overnight at 4°C in solutions containing the following primary antibodies: mouse monoclonal anti-GFAP antibody (Dako, Glostrup, Denmark); mouse monoclonal anti-Aβ antibody (82E1; IBL, Gunma, Japan); anti-EEA1; rabbit polyclonal anti-Rab4 antibody (Santa Cruz Biotechnology); rabbit polyclonal anti-Rab5 antibody (Santa Cruz Biotechnology); and rabbit polyclonal anti-Rab7 antibody (Santa Cruz Biotechnology). Sections were then incubated with AlexaFluor 568-conjugated goat anti-rabbit IgG (Invitrogen, Carlsbad, California, USA); AlexaFluor 488-conjugated goat anti-mouse IgG (Invitrogen); and DAPI nuclear stain (Santa Cruz Biotechnology) for 1 h at room temperature. For triple immunohistochemistry, anti-GFAP was prelabeled using a Zenon AlexaFluor 405 anti-mouse IgG1 kit (Invitrogen). All sections were examined using a Digital Eclipse C1 confocal microscope (Nikon, Kanagawa, Japan).

Cell cultures

Rat and cynomolgus monkey astrocyte cultures were prepared as described [12]. Cells were maintained in Dulbecco's modified Eagle's medium with 10% fetal calf serum. For western blot analyses, cells were plated at 2.0×10^4 cells/cm^2 onto six-well plates. For immunocytochemical studies, cells were plated at 1.0×10^4 cells/cm^2 onto two-well LAB-TEK chamber slides (Nalge Nunc, Rochester, New York, USA).

RNA interference and Aβ treatment study

For double-stranded RNA-mediated interference (RNAi) studies, siRNAs were designed carefully by Enhanced siDirect (RNAi Inc., Tokyo, Japan). We used the following short double-stranded RNAs (siRNAs) against rodent dynein heavy chain (siDHCm) and primate dynein heavy chain (siDHCp): siDHCm, 5′-GUAUCAGC ACGGAGUUUUUGG-3′ (sense) and 5′-UCAGACACGC UAGCAACGGAG-3′ (antisense); siDHCp, 5′-GAAAUCC GAAGCACUUAAAGA-3′ (sense) and 5′-UUUAAGUGC UUCGGAUUUCAG-3′ (antisense).

We also used other siRNAs to confirm their knockdown-specific effects: siDHCm2, 5′-GCCAUUCGUGAAUACC AGACC-3′ (sense) and 5′-UCUGGUAUUCACGAA UGGCCC-3′ (antisense); siDHCp2, 5′-GGUGGGUG UACAUUACGAAUU-3′ (sense) and 5′-UUCGUAAUGU ACACCCACCUG-3′ (antisense). The control siRNA had a random sequence. RNAi experiments were conducted using HilyMax lipid reagent (Wako, Osaka, Japan) according to the manufacturer's protocol.

For the Aβ treatment study, cells were treated with Aβ1-40 after 72 h of siRNA transfection at the final concentrations indicated: 1 μM for western blotting and 100 nM for immunocytochemistry (Aβ40 was not preaggregated; Peptide, Osaka, Japan). For the Aβ clearance study, cells were washed with 0.05% trypsin in PBS after 20 min of culture with Aβ. Cells were cultured another 2 h and then harvested.

Cells were lysed in a sample buffer solution containing 62.5 mM Tris-HCl (pH 6.8), 2 mM EDTA, 0.5% Triton X-100, 2% SDS, and a proteinase inhibitor cocktail to extract total cellular proteins and then subjected to western blot analyses. We used the following primary antibodies: mouse monoclonal anti-β-actin (Sigma, St Louis, Missouri, USA); mouse monoclonal anti-dynein intermediate chain (DIC) (Millipore, Temecula, California, USA); mouse monoclonal anti-Rab5 (Santa Cruz Biotechnology); anti-Aβ; rabbit polyclonal anti-dynein heavy chain (DHC) (Santa Cruz Biotechnology); and rabbit polyclonal anti-Rab7 (Sigma). Immunoreactive bands were quantified using commercially available software (Quantity One; PDI Inc., Upper Saddle River, New Jersey, USA), and one-way analyses of variance were performed, followed by the Bonferroni/Dunn post-hoc test. We conducted three independent experiments ($N = 6$ for each experimental group), duplicating each experiment.

Cells plated on chamber slides were fixed with 4% paraformaldehyde and then permeabilized with 0.5% Tween 20. After blocking with 3% BSA, cells were incubated overnight at 4°C with the following primary antibodies: anti-DIC; anti-EEA1; anti-Aβ; and rabbit polyclonal anti-LAMP1 (Abcam, Cambridge, Massachusetts, USA). Cells were then incubated with AlexaFluor-conjugated secondary antibodies and DAPI nuclear stain as mentioned above.

BDNF ELISA

We used a sandwich enzyme-linked immunosorbent assay (ELISA) to assess brain-derived neurotrophic factor (BDNF) production from astrocytes treated with Aβ. We used the Chemikine Brain-Derived Neurotrophic Factor Sandwich ELISA kit (Millipore) for our ELISA analyses according to the manufacturer's instructions. Culture media from rat and monkey astrocyte cultures were harvested and then used for the sandwich ELISA studies. We conducted three independent experiments

($N = 6$ for each experimental group), duplicating each experiment. For statistical analyses, one-way analyses of variance were performed, followed by the Bonferroni/Dunn post-hoc test. Data are shown as mean ± SD.

Results

Endocytic pathology in astrocytes of aged cynomolgus monkey brains

To determine whether endocytic pathology was present in the brains of aged cynomolgus monkeys, we immunostained brain sections from aged cynomolgus monkeys for EEA1, an early endosome marker. The intracellular accumulation of enlarged early endosomes is a characteristic feature of endocytic disturbances [1–3]. In aged cynomolgus monkey brains, EEA1 immunoreactivity was increased. We also observed enlarged early endosomes in several neural cells, confirming our previously reported observations (Fig. 1a) [5].

To assess whether age-related endocytic disturbances occur in astrocytes as well as in neurons, we double immunostained brain sections for several early endosome markers and GFAP, a marker for astrocytes. In young monkey brains, GFAP-positive astrocytes contained small granular early endosomes (Fig. 1b). By contrast, in aged monkey brains, GFAP-positive astrocytes contained numerous enlarged early endosomes (Fig. 1b). Clearly, the number of early endosomes was increased. In aged monkey brains, the immunoreactivity of Rab7, a marker for late endosome, was also increased (Fig. 1c).

Next, we performed triple immunostaining to investigate the relationship between astroglial endocytic disturbances and Aβ pathology in aged monkey brains. Although we did not find an obvious relationship between astrocytes showing endocytic pathology and SP deposition, we did observe accumulations of Aβ in enlarged early endosomes in aged monkey brains (Fig. 1d). Moreover, we observed several CAAs near astrocytes showing endocytic pathology, and some astrocytes appeared to envelop what looked like affected blood vessels (Fig. 1d).

Dynein dysfunction reproduces endocytic pathology in astrocytes

We showed previously that aging attenuates the dynein–dynactin interactions required for dynein-mediated transport and that dynein dysfunction reproduces endocytic disturbances, resulting in AD-associated pathologies such as the accumulation of intracellular Aβ in neuronal cells [4–6]. To assess whether dynein dysfunction also reproduces endocytic pathology in astrocytes, we carried out RNAi studies. As we showed previously that species differences in astrocytes exist between rodents and primates [12], we used both rat and cynomolgus monkey astrocytes. We chose DHC as the main knockdown target because it is well known that siRNAs targeting DHC also induce significant downregulation of DIC, resulting in sufficient dynein dysfunction [5,6,13].

Western blot analyses confirmed that our siRNAs successfully downregulated DIC in both rat and monkey astrocytes and that the depletion of dynein induced a significant increase in endosome-associated Rab GTPases, such as Rab5 and Rab7, as reported previously in neuronal cells (Fig. 2a–d) [5,6]. Immunocytochemistry confirmed that the depletion of dynein reproduced endocytic pathology, that is, the intracellular accumulation of enlarged early endosomes in both rat and monkey astrocytes (Fig. 2e and f).

Endocytic disturbances disrupt Aβ clearance in astrocytes

The amino acid sequence of cynomolgus monkey Aβ is completely homologous to that of humans. Thus, to model proposed pathophysiological processes in AD, we used cynomolgus monkey astrocytes to investigate whether endocytic disturbances affect astroglial functions such as Aβ clearance. After 20 min of Aβ treatment, the depletion of dynein failed to affect the amount of Aβ, as shown in western blot analyses (Fig. 3a and b). Several studies showed that astrocytes can generate Aβ *in vitro* [14]. However, our western blot system failed to recognize endogenous Aβ in monkey astrocytes, suggesting that Aβ detected in this study corresponds to Aβ taken up by astrocytes (data not shown).

We observed that Aβ clearance by astrocytes was disrupted by the depletion of dynein 2 h after Aβ depletion from culture medium (Fig. 3a and b). In control siRNA-transfected astrocytes, the amount of Aβ taken up decreased significantly 2 h after Aβ depletion (Fig. 3a and b). In contrast, in dynein-knockdown astrocytes, the amount of Aβ taken up remained high (Fig. 3a and b). Immunocytochemical analyses showed that after depleting Aβ for 2 h in control siRNA-transfected astrocytes, Aβ taken up was localized to lysosomes (Fig. 3c). In siDHCp-transfected astrocytes, Aβ taken up still remained in peripheral areas of the cell and accumulated in enlarged early endosomes, even after depleting Aβ for 2 h, as we observed in aged monkey astrocytes (Fig. 3c).

This is the first study to show that deficits in intracellular transport specifically disrupt astroglial Aβ clearance through endocytic disturbances. Besides playing a role in Aβ clearance, astrocytes also play an important role in the production of neurotrophic factors such as BDNF [15]. Moreover, several studies suggest that the impairment of BDNF signaling is associated with onset of AD [16–19]. In both rat and monkey astrocytes, we did not observe any significant changes in BDNF secretion because of dynein depletion (Fig. 3d).

Fig. 1

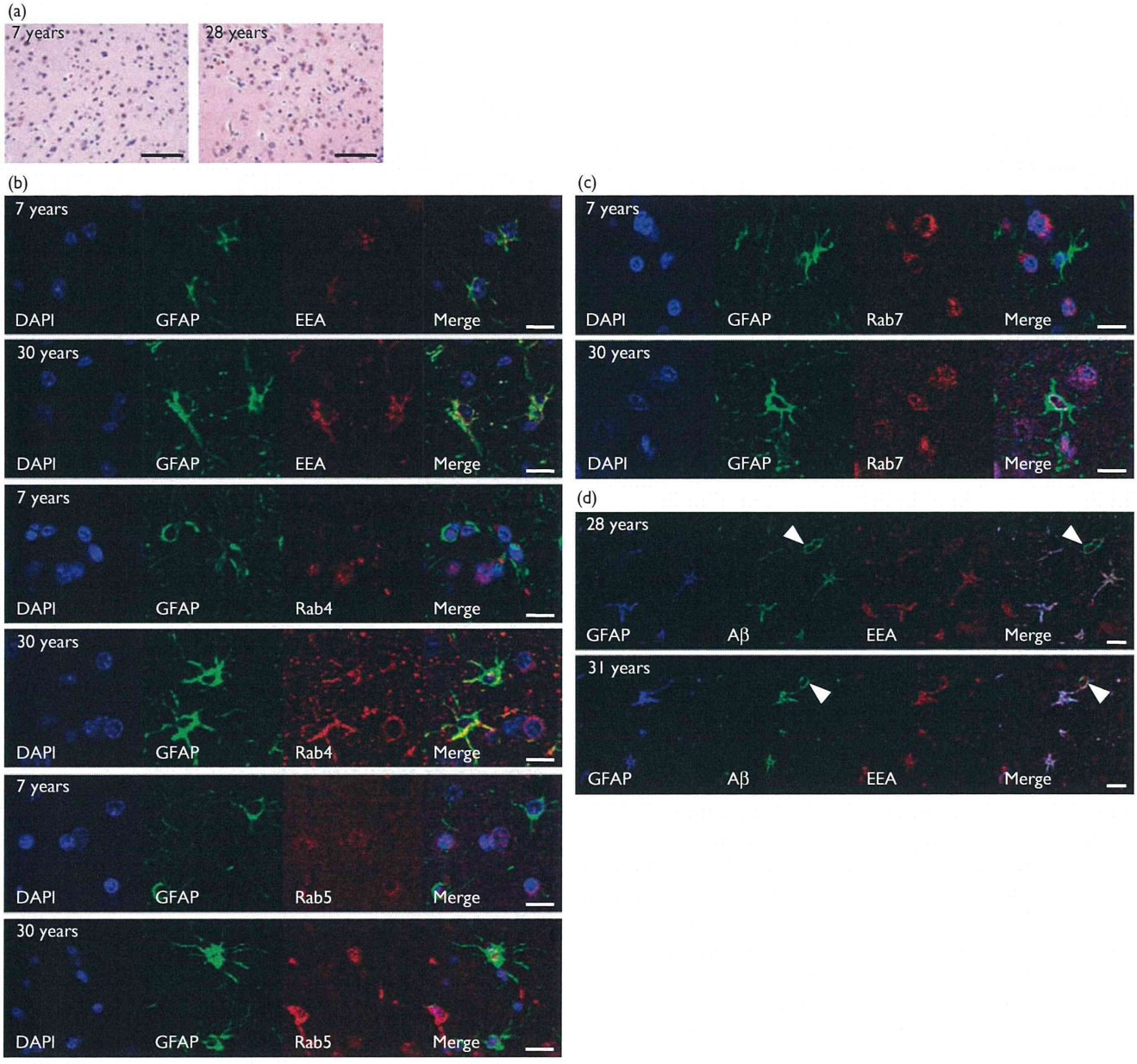

(a) Photomicrographs of temporal lobe sections from a 7-year-old (young) cynomolgus monkey and a 28-year-old (aged) cynomolgus monkey. Sections were immunostained with anti-EEA1 antibody and then counterstained with hematoxylin. In cynomolgus monkey brains, immunoreactivity against EEA1 increased with aging (scale bar, 50 μm). (b and c) Photomicrographs of temporal lobe sections from a 7-year-old monkey and a 30-year-old monkey immunostained for GFAP and early endosome markers such as EEA1, Rab4, and Rab5 (b), or late endosome marker Rab7 (c) with DAPI. In aged monkey brains, enlarged endosomes were observed within cells (scale bar, 10 μm). (d) Photomicrographs of temporal lobe sections from a 28-year-old monkey and a 31-year-old monkey. The sections were immunostained for GFAP, β-amyloid (Aβ), and EEA1. Aβ accumulated in enlarged early endosomes in astrocytes of aged monkey brains. Arrowhead shows cerebral amyloid angiopathy (scale bar, 10 μm).

Discussion

In the present study, we extended our previous findings by showing that age-related endocytic pathology also occurs in astrocytes. New observations in this study show that dynein dysfunction disrupts Aβ clearance in astrocytes through endocytic disturbances. These observations suggest that endocytic disturbances can alter astroglial functions and that they could be involved in age-related Aβ pathologies.

Our immunohistochemical analyses showed that endocytic pathology such as the intracellular accumulation of enlarged endosomes occurs even in astrocytes of aged monkey brains and Aβ accumulated in enlarged early

Fig. 2

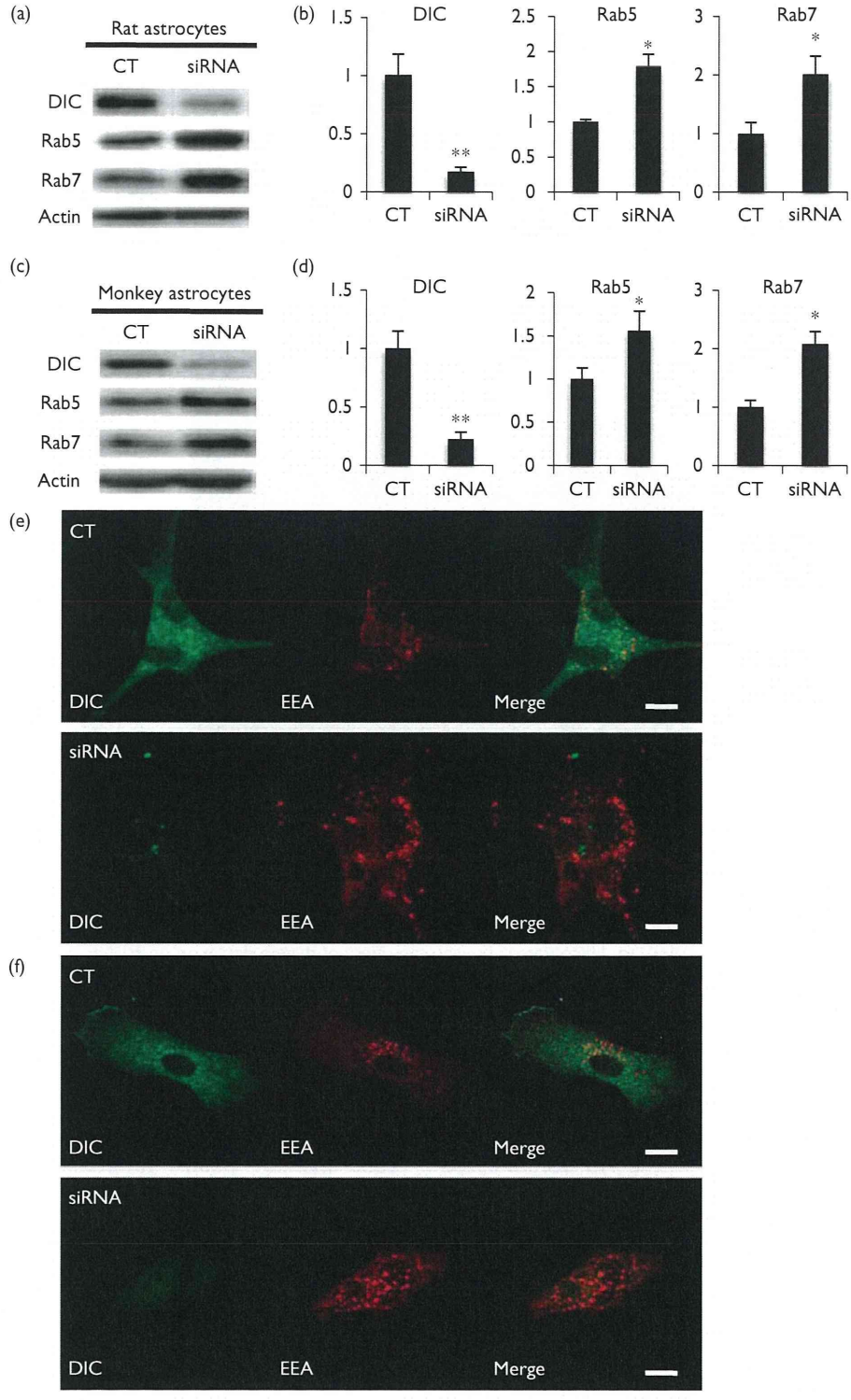

(a) Western blots showing the amount of DIC, Rab5, Rab7, and β-actin in rat astrocytes 72 h after siRNA transfection. In dynein-depleted cells, the amount of Rab5 and Rab7 was increased. (b) Histograms showing the effect of dynein depletion on the amounts of DIC, Rab5, and Rab7 in rat astrocytes. All data were normalized according to β-actin levels. Values are mean±SD (*$P<0.01$, **$P<0.001$). *Y*-axes show the mean values of the quantified data. (c) Western blots showing the amount of DIC, Rab5, Rab7, and β-actin in cynomolgus monkey astrocytes 72 h after siRNA transfection. In dynein-depleted cells, the amount of Rab5 and Rab7 was increased. (d) Histograms showing the effect of dynein depletion on the amounts of DIC, Rab5, and Rab7 in monkey astrocytes. All data were normalized according to β-actin levels. Values are mean±SD (*$P<0.01$, **$P<0.001$). *Y*-axes show the mean values of the quantified data. (e and f) Photomicrographs of rat astrocytes (e) and monkey astrocytes (f) immunostained for DIC and EEA1 72 h after siRNA transfection. In dynein-depleted cells, early endosomes were obviously enlarged and had accumulated (scale bar, 10 μm). CT, cells transfected with control siRNA; DIC, dynein intermediate chain; siRNA, cells transfected with siDHCr.